International Journal of Heat and Technology
Vol. 42, No. 4, August, 2024, pp. 1455-1464
Journal homepage: http://iieta.org/journals/ijht

Effect of Upstream Fin Length on Longitudinally Finned Flat Tubes Bank Performance Based on Constructal Design and Fuzzy Logic Control

Ahmed H. Ahmed[1*], Maki H. Zaidan[2], Manar S.M. Al-Jethelah[2]

[1] Renewable Energy Research Unit, Hawija Technical Institute, Northern Technical University, Kirkuk 34001, Iraq
[2] Department of Mechanical Engineering, College of Engineering, Tikrit University, Tikrit 34001, Iraq

Corresponding Author Email: ahmedhasan_hwj@ntu.edu.iq

https://doi.org/10.18280/ijht.420435

Received: 5 April 2024
Revised: 25 June 2024
Accepted: 10 July 2024
Available online: 31 August 2024

Keywords:
constructal design, laminar forced convection, longitudinally finned flat tubes bank heat exchanger, upstream fin length

ABSTRACT

The present study considers two-dimensional laminar incompressible flow over a longitudinally finned flat tube bank heat exchanger (*LFFTBHE*) based on the constructal design method and the Fuzzy logic control. The impact of Reynolds number (Re) and dimensionless upstream fin length (*Lu/DT*) on the *LFFTBHE* performance was studied. The finite volume method using a commercial CFD package (*ANSYS* 2022/*R2*) was used to solve the governing equations. Fuzzy logic control was used to optimize the results. The results showed that the upstream fin length insignificantly impacted the Nusselt and Bejan numbers. Increasing the dimensionless upstream fin length, i.e., from 0.4 to 1, decreased the Nusselt number up to 10.3% at Re=1200. However, the dimensionless upstream fin length increase increased the Bejan number up to 28.8% at Re=1200.

1. INTRODUCTION

A heat exchanger's performance can be evaluated by estimating the largest amount of energy transmitted and the least amount of power expended. The performance of the air side can be improved by changing the design of the fin or tube, or in some cases both due to the resistance to heat transfer from the air side is dominant. This resistance results from the low specific heat of the air and the high heat transfer coefficient on the water or the internal fluid side [1-4]. It is necessary to control the tube shape, vertical distance, horizontal distance, fin height, and the distance between the fins to reach the optimal design. All the above variables directly impact on thermal conductance or the largest value of the heat transfer coefficient, as well as the area density and the consequent cost, size, and weight, considering the metal type. The above considerations were adopted in studying forced and natural convection heat transfer to analyze the performance of tube bank heat exchangers (*TBHE*) [5-9]. Previous research in the literature suggests that the tube's form and design can improve heat exchanger design criteria, including the exterior tube heat transfer coefficient and the external flow pressure drop [10-16]. The width of the flow channel is not equal to the convective body that forms on the channel walls as a result of boundary layers because the dimensions of the flow body and the channel are different. A different strategy is to equalize the size of the flow body and flow channel. This methodology's cornerstone is the constructal design technique, based on the constructal law.

The optimal flow channel size is determined by the ease with which heat can be transferred from the walls to the air streams [17, 18]. The constructal design procedure for rhombic tubes in crossflow and three dimensionless pressure differences (Be=10^3, 10^4, and 10^5) was investigated. It was reported that at any dimensionless pressure difference, the maximal heat transfer density was higher for narrower rhombic tubes [19]. To enhance the density of heat transfer, a vertical array of flat tubes in cross-flow with a fixed pressure drop was investigated. The maximum heat transfer densities of naturally chilled tubes with varying cross-sectional areas were reported [20, 21]. Other studies were investigated the maximum heat transfer densities from multiscale tubes and fins in forced and natural convection [22-26]. The thermal fluid properties in two dimensions over two staggered flat tubes and the thermal fluid characteristics across a tube series between two parallel plates were studied. As was already indicated, studies suggested a proportional relationship between the Re and Nu [27-32]. A semicircular segment of a tube placed in a crossflow at different angles was numerically and experimentally investigated. the studied Re ranged from 2200 and 45000. The greatest Nu number was at the arc's surface, which was normal to the flow direction (zero angle of attack) [33]. The airflow turbulence in an elliptic tube bundle has been studied using experimental and computational fluid dynamics models. The Reynolds number range examined was $5600 \leq Re \leq 40000$. Tests were conducted with an air angle of attack ranging from 0° to150°, and the four-axis ratios of the tube were 0.25, 0.33, 0.5, and 1. The lowest thermal performance was at 90°, and the highest was at 0° [34]. Heat transfer and pressure drop through finned flat plate banks was investigated for Pr=0.71 and $124 \leq Re \leq 1238$. As Re increased from 124 to 1238, Nu increased from 113.6% to 150.3%, and the friction factor decreased 57.7% [35]. A numerical investigation studied the impact of Re and the fin

pitch on the thermal and hydraulic performance of finned-tube heat exchanger. Increasing Re from 750 to 2350 increased the heat transfer rate by 84% at fin pitch of 20 mm. At Re=2350, increasing the fin pitch from 7.5 mm to 20 mm increased the heat rate by 100%. It was found that the j factor decreased by 34% when Re increased from 750 to 2350 at fin pitch of 20mm. At Re=2350, the j factor increased 12% as the fin pitch increased from 7.5 mm to 20 mm [36]. The impact of a wavy fin on the thermal behavior of a heat exchanger was numerically studied [37]. It was found that the heat transfer coefficient decreased by 23% at fin pitch of 1.2mm and 11.5% at 2.0 mm.

Heat transfer and crossflow air in a staggered configuration of flat tube heat exchangers were experimentally studied [38]. The air attack angles and tube aspect ratios effect were investigated. The analysis covers a range of air velocities from 2 to 6 m/s and includes 19 heat exchanger cases with six attack angles from 0 to 150° with a 30° step and four aspect ratios: 0.18, 0.39, 0.66, and 1. The results showed that the pressure drop and thermal performance were controlled by the tube aspect ratios and attack angles. The Neuro-fuzzy inference system model was employed to predict the heat transfer coefficient and pressure drop values [39]. Three longitudinal pitches (3, 4, and 6) and transverse pitches from 1.5 to 4.5 with a step of 1.0 were investigated for Reynolds numbers ranged from 10 to 320. The average discrepancy between the numerical and ANFIS model values for the average Nu was 1.9%, and the dimensionless pressure drop was 2.97%.

The previous investigations conducted numerical and experimental studies on identically shaped tubes, i.e., cylindrical and elliptic, for inline and staggered flattened tube configurations. In the studies mentioned above, the constructal design for *LFFTBHE* was not considered. Also, the present study introduces a fuzzy logic control of *LFFTBHE* in crossflow. The present work studied the impact of upstream length at $200 \leq Re \leq 1200$ on Nu and Be numbers. The studied fluid was air, Pr=0.7108. The tube was maintained at a constant surface temperature. Four dimensionless upstream fin lengths (*Lu/DT*) (0.4, 0.6, 0.8, and 1) were considered. The objective function of the present investigation is to maximize heat transfer rate, i.e., Nu number, and minimize the pressure drop, i.e., Be number.

2. MATHEMATICAL MODELLING

The air-side physical model of LFFTBHE, shown in Figure 1, was considered to study its heat transfer performance. Usually, this kind of heat exchanger has a large number of LFFT. The following assumptions were applied: a steady state, laminar flow, constant surface temperature, incompressible fluid, no viscous dissipation, and constant thermophysical properties of the working fluid. The airflow was heated by convection heat transfer caused by the horizontal x-y plane. The two-dimensional governing equations that describe the flow and heat transfer fields are given below [40, 41]:
Continuity equation:

$$\frac{\partial u}{\partial x}+\frac{\partial v}{\partial y}=0 \tag{1}$$

Momentums equations in the x- and y- directions:

$$\rho\left(u\frac{\partial u}{\partial x}+v\frac{\partial u}{\partial y}\right)=-\frac{\partial p}{\partial x}+\mu\left(\frac{\partial^2 u}{\partial x^2}+\frac{\partial^2 u}{\partial y^2}\right) \tag{2}$$

$$\rho\left(u\frac{\partial v}{\partial x}+v\frac{\partial v}{\partial y}\right)=-\frac{\partial p}{\partial y}+\mu\left(\frac{\partial^2 v}{\partial x^2}+\frac{\partial^2 v}{\partial y^2}\right) \tag{3}$$

Energy equation:

$$\left(u\frac{\partial T}{\partial x}+v\frac{\partial T}{\partial y}\right)=\alpha\left(\frac{\partial^2 T}{\partial x^2}+\frac{\partial^2 T}{\partial y^2}\right) \tag{4}$$

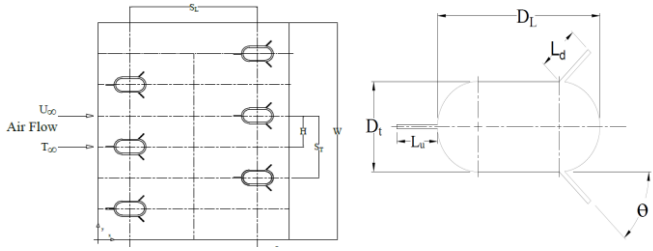

Figure 1. Rows of *LFFTBHE* in crossflow

Eqs. (1) to (4) can be non-dimensionalized using the following dimensionless forms:

$$X,Y=\frac{x,y}{Dt},\ U,V=\frac{u,v}{(\Delta p/\rho)^{\frac{1}{2}}},\ P=\frac{p}{p_{in}-p_{out}},\quad \theta=\frac{T-T_o}{T_w-T_o},\ Pr=\frac{\mu Cp}{K} \tag{5}$$

Now, with the above dimensionless variables in Eq. (5), Eqs. (1)-(4) become:

$$\frac{\partial U}{\partial X}+\frac{\partial V}{\partial Y}=0 \tag{6}$$

$$U\frac{\partial U}{\partial X}+V\frac{\partial U}{\partial Y}=-\frac{\partial P}{\partial X}+\sqrt{\frac{Pr}{Be}}\left(\frac{\partial^2 U}{\partial X^2}+\frac{\partial^2 U}{\partial Y^2}\right) \tag{7}$$

$$U\frac{\partial V}{\partial X}+V\frac{\partial V}{\partial Y}=-\frac{\partial P}{\partial X}+\sqrt{\frac{Pr}{Be}}\left(\frac{\partial^2 V}{\partial X^2}+\frac{\partial^2 V}{\partial Y^2}\right) \tag{8}$$

$$U\frac{\partial \theta}{\partial X}+V\frac{\partial \theta}{\partial Y}=\frac{1}{\sqrt{(\mathrm{BePr})}}\left(\frac{\partial^2 \theta}{\partial X^2}+\frac{\partial^2 \theta}{\partial Y^2}\right) \tag{9}$$

The key dimensionless numbers, i.e., Re, Be, and Nu, are defined as:

$$Re=\frac{\rho \mathrm{VD}}{\mu},Be=\frac{\Delta p DT^2}{\mu\alpha},\mathrm{Nu}=\frac{\mathrm{h\ D}_h}{k} \tag{10}$$

The average Nu can be defined as:

$$\mathrm{Nu}=\frac{1}{s}\int -\left.\frac{\partial\theta}{\partial n}\right|_s ds \tag{11}$$

Other dimensionless parameters are normalized by the transverse tube diameter (*DT*), as the upstream fin length=(*Lu*/*DT*), transverse pitch ratio=(*ST*/*DT*), the longitudinal pitch=(*SL*/*DT*), downstream fin length (*Ld*/*DT*), dimensionless fin angle $\theta ds=\theta\pi/180$.

Figure 2 displays the computing domain and the concept of

staggered tube banks. The applied boundary conditions are as follows:

$$\text{A:} \quad \frac{\partial U}{\partial Y} = 0, V = 0, \frac{\partial \theta}{\partial Y} = 0 \tag{12}$$

$$\text{B:} \quad U = 1, \frac{\partial V}{\partial X} = 0, \theta = 0 \tag{13}$$

$$\text{C:} \quad \frac{\partial U}{\partial X} = \frac{\partial V}{\partial X} = 0, \frac{\partial \theta}{\partial X} = 0 \tag{14}$$

$$\text{D:} \quad U = V = 0, \theta = 1 \tag{15}$$

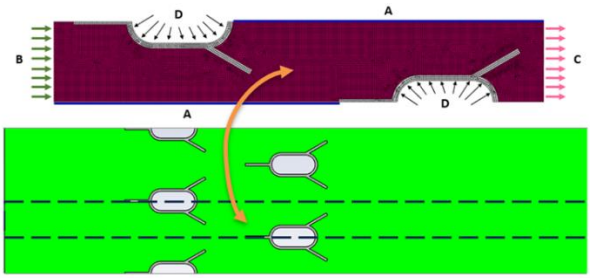

Figure 2. Boundary conditions around and on LFFTBHE in crossflow

3. NUMERICAL SIMULATION

The present problem was numerically solved using a control-volume-based finite volume approach (Fluent-CFD) software solver was used to solve the governing equations under the assumed boundary conditions. To interpolate the convection fluxes, upwind differencing scheme, hybrid scheme, and central differencing Scheme were employed. SIMPLE algorithm was used in pressure-velocity coupling. The maximum residue permitted for convergence check was 10^8. Figure 3 presents the model flowchart.

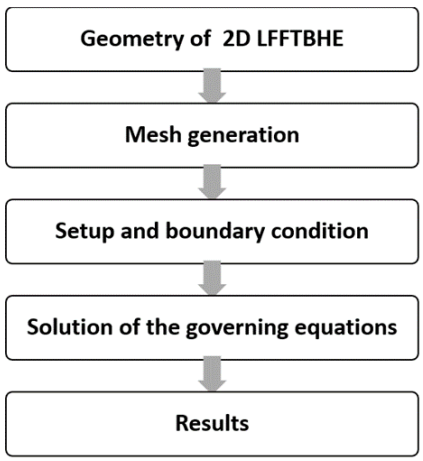

Figure 3. Model flowchart

4. GRID GENERATION VALIDATION OF THE COMPUTATIONAL MODEL

The entire studied computational domain was discretized with more than 45000 unstructured mesh elements. Quadratic element order was selected. The solver has a size of $0.01mm$ for the entire computational domain and a smooth inflation transition near tube and fin surfaces.

Code validation is an essential part of any numerical investigation [42, 43]. The validation of the computational code ($ANSYS\ FLUENT\ 2022/R2$) for test problems and predictions was performed using the developed code with exact solutions and experimental data, as well as the standard issues available in previous studies. The numerical predictions established in this study were compared with those in the literature under similar tube conditions. The Re numbers of $10 \leq Re \leq 100$ were adopted to predict the average Nu number. Comparison with previous experimental results was performed to validate the present numerical results obtained through the finite volume codes for the flat shape in the staggered arrangement. The completion of the code validation was based on the overall heat transfer rate. Figure 4 presents a comparison between the present simulation results and [44]. The deviation increased with Re. The maximum deviation values were approximately 2.62% and 2.48% for Re 10 and 100, respectively. These deviations appeared due to ignoring the dimensionless temperature at the inlet and outlet of heat exchanger modules, as well as the influence of the changes in thermal properties with temperature and the approximate thermal properties.

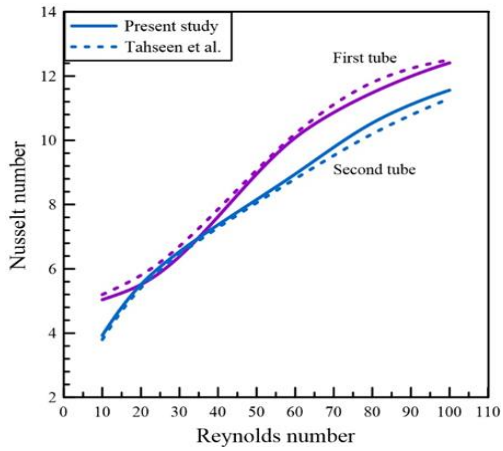

Figure 4. Comparison between the present study with [44] for average Nusselt Number with Reynolds number

5. FUZZY LOGIC CONTROL

Since the 1960s, fuzzy logic has been utilized more and more in control research. The extension of well-known Boolean logic methods serves as the basis for the fuzzy logic [45]. Analyzing the mathematical model dynamics of a physical process using fuzzy logic and arbitrary order has been extensively studied in the last few decades [46]. Applications of fuzzy logic aid in solving issues about measuring uncertainty in mathematical disease modeling. A model with a triangle membership function based on a specific population was calculated, and the fuzzy reproduction number and fuzzy equilibrium points were found. The primary *LFFTBHE* parameters are suggested to be controlled by the fuzzy logic in this work. First, the system's mathematical model was used to calculate the pressure drop, Bejan Number, Nusselt Number, and heat transfer rate. For simple and complicated systems, the fuzzy logic serves as monitor and processing tools. The membership functions were used to translate the steps of fuzzification and defuzzification. The input and output values

were first transformed from crisp to fuzzy, i.e., a process known as fuzzification, and then from Fuzzy to crisp once again to finish this translation, i.e., a process known as defuzzification.

Table 1. The input/ output ranges of data

I/P	Min	Max	O/P	Min.	Max.
$\widehat{Lu}$	0.4	1	Be	4220281.79	118042599.50
Re	200	1200	Nu	7.22	15.65
			P_{ds}	8.04	9.29
			$\hat{Q}$	134.04	271.28

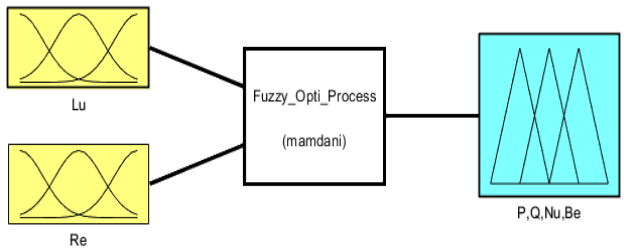

(a)

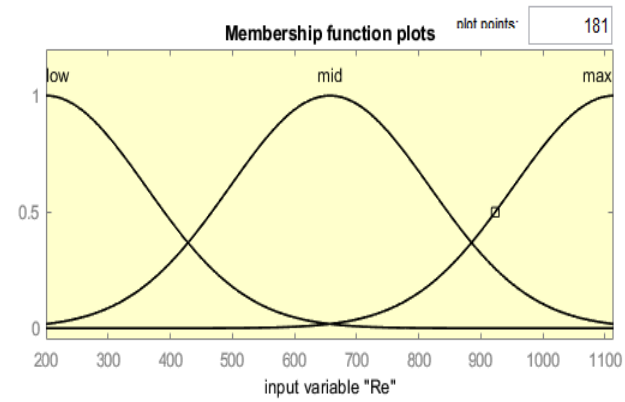

(b)

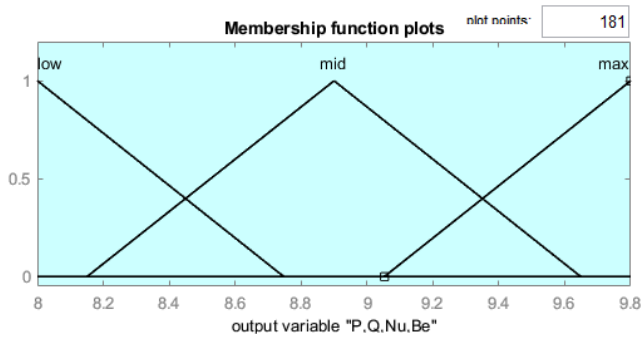

(c)

Figure 5. Fuzzy model and member ships

A summary of the input/output data is provided in Table 1. Figure 5(a) illustrates how the input parameter (fuzzification) directly affects the output (defuzzification). A particular range of data for each input is anticipated during the mathematical module, which has already been completed in the present work. The data type represented in the Fuzzification process, which turns numerical values into linguistic variables, is the membership function (MF), which is 3D. For every input, three preset values represent the overall levels of any range, i.e., low, medium, and high. The transition form used in this work is of the Gaussian type, which is close to the actual input and output parameters shown in Figure 5(b)-(c).

Because it illustrates the time shift between the two levels of the variables, the overlap between the *MF*s is crucial. The y-intercept is set at zero. However, the y-delta is low, mid, and high. There is a nonlinear transition between the parameter values. For a nonlinear operation closest to reality, the *MF* is fixed at three for each input variable and of Gaussian type [47]. The primary processor for the present work is the Mamdani inference system. If the parameters in the *LFFTBHE* have a certain value, which results in a particular value for the answers. Since responses are the primary regulated parameter in this project, the rules coded into the inference system should consider the ideal level of outputs.

6. RESULTS AND DISCUSSION

The numerical solutions for laminar forced convection heat transfer across *LFFTBHE*, based on fuzzy logic control and the constructal design method, are presented in this section. The optimum of the staggered finned flat tubes at a fixed volume was considered concerning the upstream fin length variable, and the other parameters were constant. The dimensions of the fixed volume are presented in Figure 6.

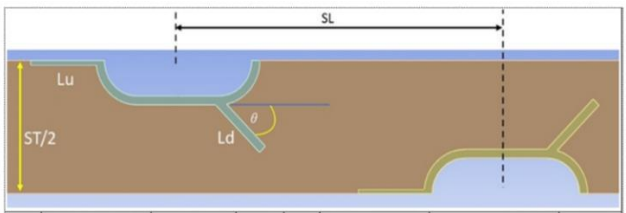

NO	PARAMETERS	SCALE	UNIT	NO	PARAMETERS	SCALE	UNIT
1	ST	30	mm	5	Ld	8	mm
2	SL	40	mm	6	θ	30^0	DEGRE
3	Lu	VARIABLE	mm	7	Re	$200 \leq Re \leq 1200$	
4	T_s	90	℃	8	T_∞	25	℃

Figure 6. Geometric parameters of *LFFTBHE* arrangements

Figure 7 shows the upstream fin length effect on the temperature and velocity contours $0.4 \leq Lu/DT \leq 1$ with $SL/DT = 4$, $ST/DT = 3$, $Ld/DT = 0.8$, $\theta = 0.53$, and $200 \leq Re \leq 1200$. The flow separation occurred when the fluid collides with the upstream fin length. The fluid angle begins to expand relatively with the upstream fin length. The fluid moves away from the front of the $LFFTBHE$. In other words, the adjacent layer grows continuously along the front interface, even at a high Reynolds number. A distinct region is established between the body and the fluid stream when a fluid detaches from a body. The segregated region, a low-pressure zone located behind the body, is the site of recirculation and backflows. The pressure drag is directly affected by the size of the separation zone. A bigger separated region results in a higher pressure drag. The downstream effects of the flow separation are characterized by a decrease in velocity in comparison to the upstream velocity. The wake is the term used to describe the trailing region of flow, where the body's influence on velocity is readily apparent. The region separated is concluded upon the reconnection of the two flow streams.

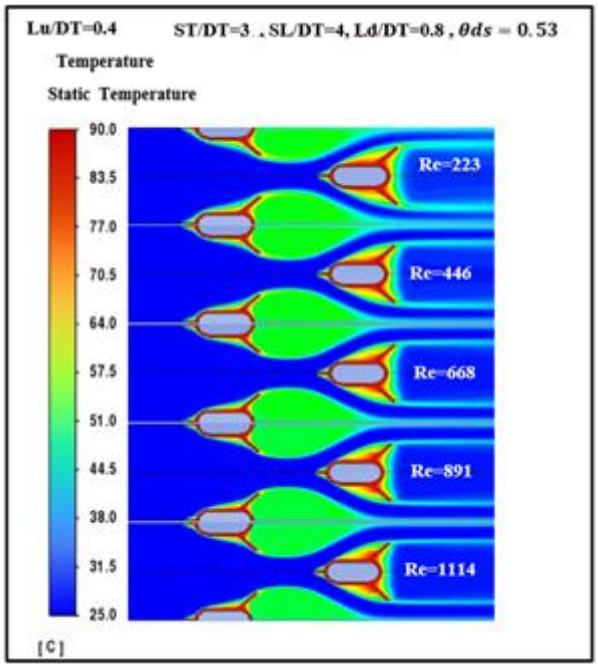
Lu/DT=0.4
ST/DT=3 , SL/DT=4, Ld/DT=0.8 , θds = 0.53
Temperature
Static Temperature
90.0
83.5
77.0
70.5
64.0
57.5
51.0
44.5
38.0
31.5
25.0
[C]
Re=223
Re=446
Re=668
Re=891
Re=1114

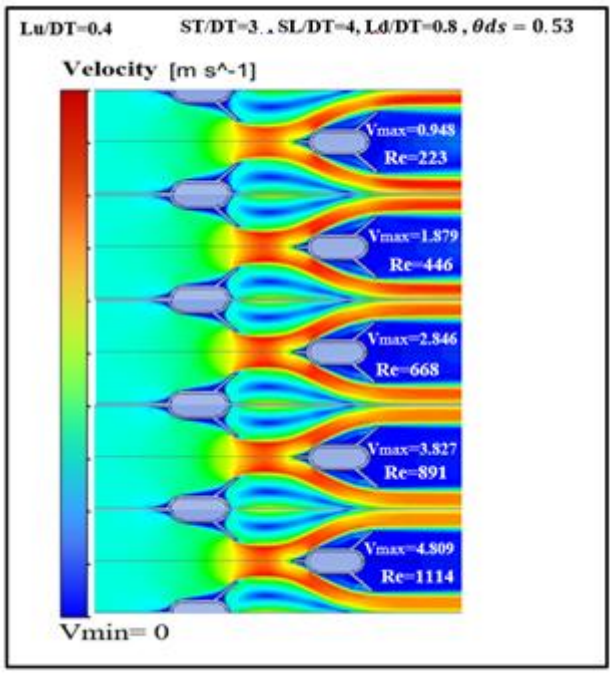
Lu/DT=0.4
ST/DT=3 , SL/DT=4, Ld/DT=0.8 , θds = 0.53
Velocity [m s^-1]
Vmax=0.948
Re=223
Vmax=1.879
Re=446
Vmax=2.846
Re=668
Vmax=3.827
Re=891
Vmax=4.809
Re=1114
Vmin= 0

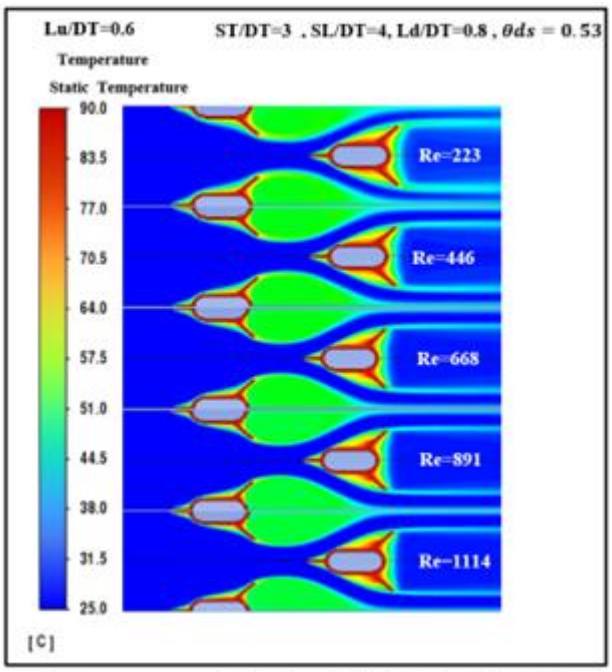
Lu/DT=0.6
ST/DT=3 , SL/DT=4, Ld/DT=0.8 , θds = 0.53
Temperature
Static Temperature
90.0
83.5
77.0
70.5
64.0
57.5
51.0
44.5
38.0
31.5
25.0
[C]
Re=223
Re=446
Re=668
Re=891
Re=1114

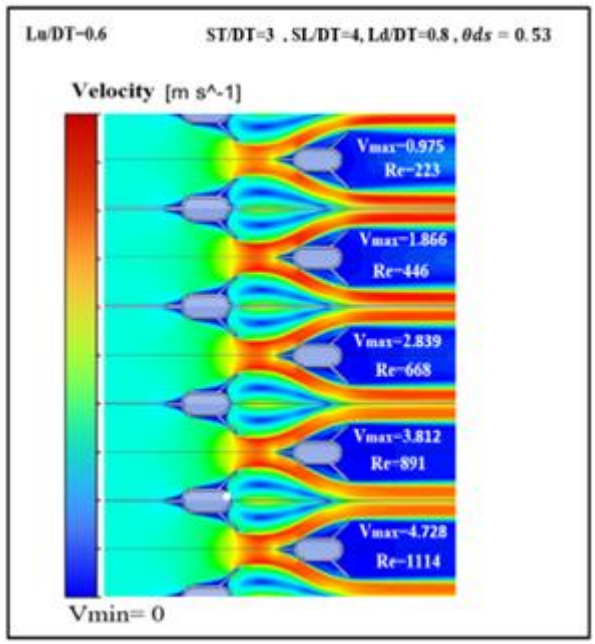
Lu/DT=0.6
ST/DT=3 , SL/DT=4, Ld/DT=0.8 , θds = 0.53
Velocity [m s^-1]
Vmax=0.975
Re=223
Vmax=1.866
Re=446
Vmax=2.839
Re=668
Vmax=3.812
Re=891
Vmax=4.728
Re=1114
Vmin= 0

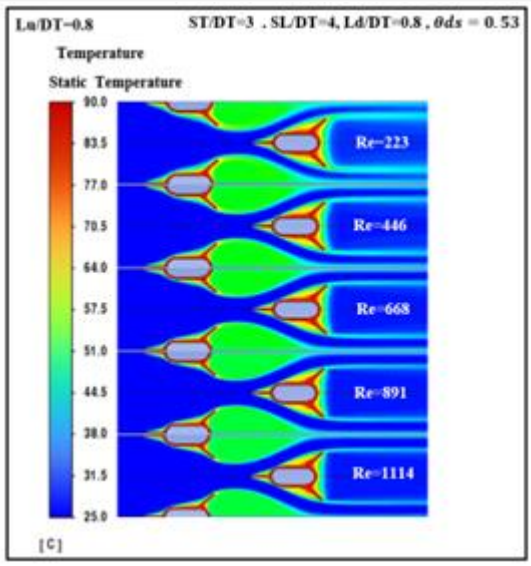
Lu/DT=0.8
ST/DT=3 , SL/DT=4, Ld/DT=0.8 , θds = 0.53
Temperature
Static Temperature
90.0
83.5
77.0
70.5
64.0
57.5
51.0
44.5
38.0
31.5
25.0
[C]
Re=223
Re=446
Re=668
Re=891
Re=1114

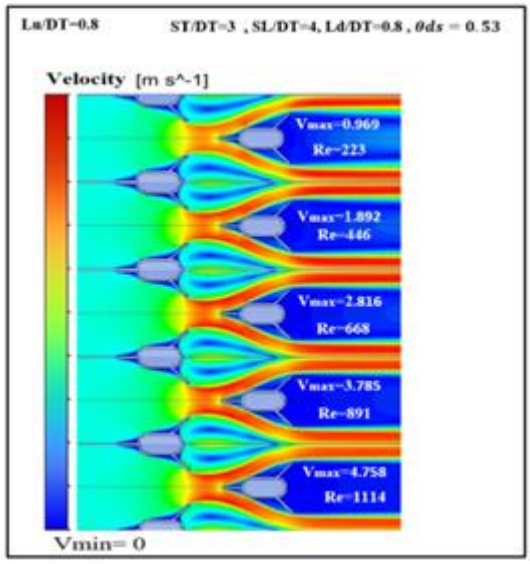
Lu/DT=0.8
ST/DT=3 , SL/DT=4, Ld/DT=0.8 , θds = 0.53
Velocity [m s^-1]
Vmax=0.969
Re=223
Vmax=1.892
Re=446
Vmax=2.816
Re=668
Vmax=3.785
Re=891
Vmax=4.758
Re=1114
Vmin= 0

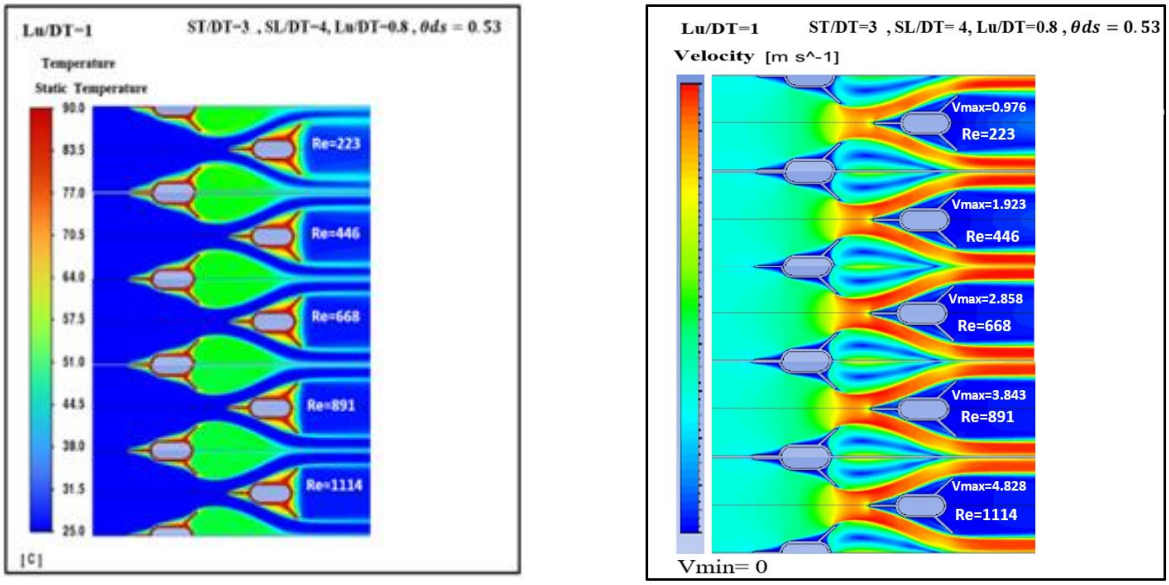

Figure 7. Temperature and velocity contours for $0.4 \leq \frac{Lu}{DT} \leq 1$ with $\frac{SL}{DT} = 4, \frac{ST}{DT} = 3, \frac{Ld}{DT} = 0.8, \theta = 0.53, and\ 200 \leq Re \leq 1200$

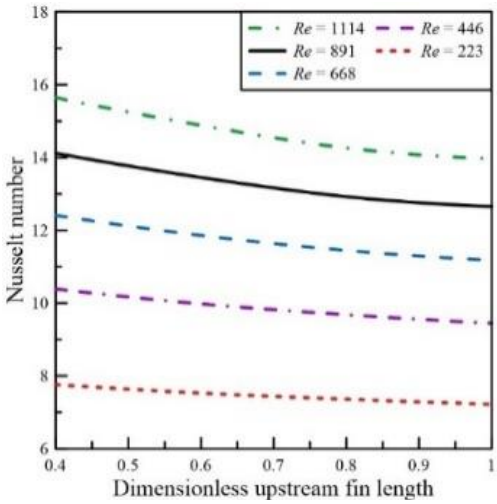

Figure 8. Nusselt number against dimensionless upstream fin length for various Reynolds numbers

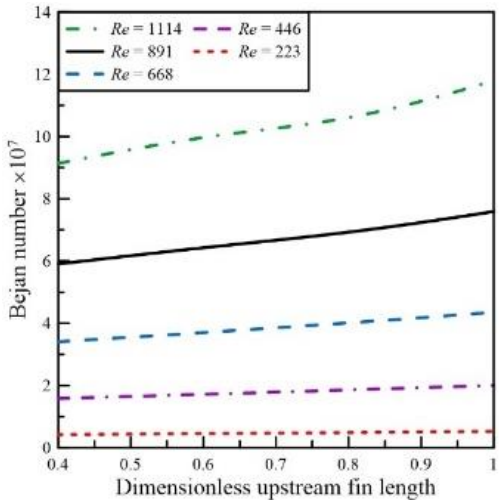

Figure 10. Bejan number against dimensionless upstream fin length for various Reynolds numbers

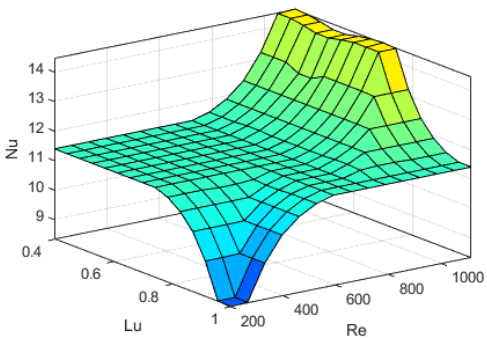

Figure 9. Reynolds number and dimensionless upstream fin length against Nusselt number

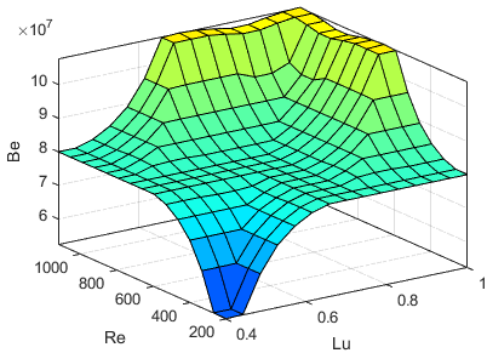

Figure 11. Reynolds number and dimensionless upstream fin length against Bejan number

The divided area is therefore an enclosed volume. Simultaneously, the wake keeps growing behind the body until the wake region fluid returns to its original velocity, and the velocity profile almost flattens out once more. Viscous and rotational effects play a crucial role in the boundary layer, the separated region, and the wake [48, 49].

Figures 8 and 9 show the impact of the upstream fin length on the Nusselt number for various Reynolds numbers. The Nusselt is inversely proportional to the upstream fin length. At Re=200, Nu was 7.7 and 7.2 at 0.4 and 1 dimensionless upstream fin length. At Re=1200, Nu was 15.6 and 14.0 at 0.4 and 1 dimensionless upstream fin length. The main reason for

this phenomenon is the separation of the fluid in the first stages, which prevents it from colliding with the upstream fin. The adjacent layer grows due to the absence of the effect of fluid momentum, which prevents it from sweeping the adjoining layer. This process is accompanied by an increase in thermal insulation between the surface of the pipe and the fluid. As a result, the heat transfer between the fluid and the surface decreases. This result is consistent with references [33, 50]. Nu increased 101% with Re from 200 to 1200 at 0.4 dimensionless upstream fin length. While Nu 92.8% with Re from 200 to 1200 at 1 dimensionless upstream fin length. The increase in Nu value with Re is due to increasing the flow mixing. In other words, the dimensionless heat transfer coefficient increases with mass flow rate, which agrees with [51]. Figures 10 and 11 show the impact of the dimensionless upstream fin length on the Bejan number for various Reynolds numbers. Be increased from 0.45×10^7 to 0.56×10^7 as the dimensionless upstream fin length increased from 0.4 to 1 at Re=200. Be increased from 9.24×107 to 11.9×107 as the dimensionless upstream fin length increased from 0.4 to 1 at Re=1200. Referring to the velocity contour and observing the up-stream fin length fluid flow lines thoroughly explains the turbulence process or not depending on the up-stream fin length. In addition, the fluid colliding with the front of the fin almost completely cancels the momentum resulting from the collision, or rather, it disappears relatively as the upstream fin length increases. The fluid tends to fill the space between the tubes, so friction begins to decrease relatively, accompanied by a clear decrease in the pressure drop. This process is accompanied by an increase in the speed of the fluid displaced between the rows of the heat exchanger to collide with the upstream fins. Therefore, the pressure drop gained can be considered a result of this procedure.

The findings of the present study in terms of increasing the heat transfer and reduce the pressure drop could be valuable for heat exchangers in several applications, such as automobiles and generators.

7. CONCLUSION

The construction and validation of a two-dimensional numerical model of a *LFFTBHE* have been completed successfully utilizing the constructal design approach. The results obtained showed the behavior of the heat transfer density as a function various dimensionless upstream fin length for $0.4\leq Lu/DT\leq1$ and $200\leq Re\leq1200$. The following conclusions have been attained as an outcome of the present study.

i. As the upstream fin length increase, the fluid flow separation increased. While the upstream fin length insignificantly impacted the isothermal contours.
ii. Optimal heat transfer was achieved for the investigated operating conditions and heat exchanger geometry at the lowest dimensionless upstream fin length and corresponding to the highest value of the Reynolds number.
iii. At $Lu/DT = 0.4$, more heat could be transferred as Nu reached 15.6.
iv. The Bejan number increased with the dimensionless upstream fin length for any Reynolds. The highest Bejan number reached was 11.9×10^7 at the dimensionless upstream fin length of 1 and Re=1.
v. Lastly, as the upstream fin length rises, the average Nusselt number drops.
vi. Future studies should further investigate the achievements of the present study by surveying and changing the back diameter of the tube by fixing the other side with the optimal arrangement (i.e., cam-finned tube).

ACKNOWLEDGMENTS

The authors thank the Faculty of Mechanical Engineering at Tikrit University and Northern Technical University, Technical Institute, Renewable Energy Research Unit, Hawija, Iraq.

REFERENCES

[1] Chen, C.J., Wung, T.S. (1989). Finite analytic solution of convective heat transfer for tube arrays in crossflow: Part II-heat transfer analysis. Journal of Heat Transfer, 111(3): 641-648. https://doi.org/10.1115/1.3250730

[2] Wu, Z., You, S., Zhang, H., Zheng, W. (2020). A comparative experimental study on the performance of staggered tube-bundle heat exchanger with unequally-pitch and equally-pitch arrangement in oscillating flow. International Journal of Heat and Mass Transfer, 154: 119680. https://doi.org/10.1016/j.ijheatmasstransfer.2020.119680

[3] Ibrahim, T.K., Al-Sammarraie, A.T., Al-Jethelah, M.S.M., Al-Doori, W.H., Salimpour, M.R., Tao, H. (2020). The impact of square shape perforations on the enhanced heat transfer from fins: Experimental and numerical study. International Journal of Thermal Sciences, 149: 106144. https://doi.org/10.1016/j.ijthermalsci.2019.106144

[4] Eleiwi, M.A., Tahseen, T.A., Hameed, A.F. (2020). Numerical study of fluid flow and heat transfer in a backward facing step with three adiabatic circular cylinder. Journal of Advanced Research in Fluid Mechanics and Thermal Sciences, 72(1): 80-93. https://doi.org/10.37934/arfmts.72.1.8093

[5] Eleiwi, M.A., Tahseen, T.A., Ghareeb, A.H. (2020). Intelligent control based estimation of heat transfer coefficient from four flat tubes with different attack air angles. Journal of Advanced Research in Fluid Mechanics and Thermal Sciences, 72(2): 65-78. https://doi.org/10.37934/arfmts.72.2.6578

[6] Bejan, A., Lorente, S. (2008). Design with Constructal Theory. John Wiley & Sons, Inc. https://doi.org/10.1002/9780470432709

[7] Lorente, S., Bejan, A. (2019). Current trends in constructal law and evolutionary design. Heat Transfer-Asian Research, 48(8): 3574-3589. https://doi.org/10.1002/htj.21556

[8] Mustafa, A.W. (2018). Maximization of heat transfer density rate from a single row of rhombic tubes cooled by forced convection based on constructal design. Heat Transfer-Asian Research, 48(2): 624-643. https://doi.org/10.1002/htj.21398

[9] Mustafa, A.W., Ghani, I.A. (2019). Maximization of heat transfer density from a vertical array of flat tubes in cross flow under fixed pressure drop using constructal design.

Heat Transfer-Asian Research, 48(8): 3489-3507. https://doi.org/10.1002/htj.21551
[10] Mustafa, A.W. (2018). Maximization of heat transfer density rate from a single row of rhombic tubes cooled by forced convection based on constructal design. Heat Transfer-Asian Research, 48(2): 624-643. https://doi.org/10.1002/htj.21398
[11] Mustafa, A.W. (2019). Constructal design of multi-scale diamond-shaped pin fins cooled by mixed convection. International Journal of Thermal Sciences, 145: 106018. https://doi.org/10.1016/j.ijthermalsci.2019.106018
[12] Mustafa, A.W., Suffer, K.H., Filaih, A.B. (2020). Constructal design of flat tubes cooled by natural convection. Heat Transfer, 50(3): 2049-2063. https://doi.org/10.1002/htj.21968
[13] Bello-Ochende, T., Bejan, A. (2005). Constructal multi-scale cylinders in cross-flow. International Journal of Heat and Mass Transfer, 48(7): 1373-1383. https://doi.org/10.1016/j.ijheatmasstransfer.2004.10.013
[14] Bello-Ochende, T., Bejan, A. (2005). Constructal multi-scale cylinders with natural convection. International Journal of Heat and Mass Transfer, 48(21-22): 4300-4306. https://doi.org/10.1016/j.ijheatmasstransfer.2005.05.023
[15] Mohammed Al-Jewaree, H. (2018). An experimentally investigate the fin thermal performance to the different fin spaces by natural convections. Al-Kitab Journal for Pure Science, 2(1): 1-13. https://doi.org/10.32441/kjps.v2i1.129
[16] Refaat, L., Hussein, A. (2018). Heat transfer enhancement of alumina nanofluid flow in a Circular tube. Al-Kitab Journal for Pure Sciences, 2(1). https://doi.org/10.32441/kjps.v2i1.130
[17] Mustafa, A.W. (2019). Constructal design of multi-scale diamond-shaped pin fins cooled by mixed convection. International Journal of Thermal Sciences, 145: 106018. https://doi.org/10.1016/j.ijthermalsci.2019.106018
[18] Waheed Mustafa, A., Hussein Abdul Elqadir, H. (2020). Constructal design of multiscale elliptic tubes in crossflow. Heat Transfer, 49(4): 2059-2079. https://doi.org/10.1002/htj.21708
[19] Page, L.G., Bello-Ochende, T., Meyer, J.P. (2013). Constructal multi scale cylinders with rotation cooled by natural convection. International Journal of Heat and Mass Transfer, 57(1): 345-355. https://doi.org/10.1016/j.ijheatmasstransfer.2012.10.048
[20] Tahseen, T.A., Ishak, M., Rahman, M.M. (2012). Analysis of laminar forced convection of air for crossflow over two staggered flat tubes. International Journal of Automotive and Mechanical Engineering, 6: 755-767. https://doi.org/10.15282/ijame.6.2012.7.0061
[21] Tahseen, T.A., Ishak, M., Rahman, M.M. (2014). An experimental study of heat transfer and friction factor characteristics of finned flat tube banks with in-line tubes configurations. Applied Mechanics and Materials, 564: 197-203. https://doi.org/10.4028/www.scientific.net/amm.564.197
[22] Tahseen, T.A., Ishak, M., Rahman, M.M. (2015). An overview on thermal and fluid flow characteristics in a plain plate finned and un-finned tube banks heat exchanger. Renewable and Sustainable Energy Reviews, 43: 363-380. https://doi.org/10.1016/j.rser.2014.10.070
[23] Jassim, A.H., Tahseen, T.A., Mustafa, A.W., Rahman, M.M., Ishak, M. (2019). An experimental investigation in forced convective heat transfer and friction factor of air flow over aligned round and flattened tube banks. Heat Transfer-Asian Research, 48(6): 2350-2369. https://doi.org/10.1002/htj.21496
[24] Toolthaisong, S., Kasayapanand, N. (2013). Effect of attack angles on air side thermal and pressure drop of the cross flow heat exchangers with staggered tube arrangement. Energy Procedia, 34: 417-429. https://doi.org/10.1016/j.egypro.2013.06.770
[25] Tahseen, T.A., Ishak, M., Rahman, M.M. (2014). Performance predictions of laminar heat transfer and pressure drop in an in-line flat tube bundle using an adaptive neuro-fuzzy inference system (ANFIS) model. International Communications in Heat and Mass Transfer, 50: 85-97. https://doi.org/10.1016/j.icheatmasstransfer.2013.11.007
[26] Bender, E. (1981). Numerical heat transfer and fluid flow. Von S. V. Patankar. Hemisphere Publishing Corporation, Washington – New York – London. McGraw Hill Book Company, New York 1980. 1. Aufl., 197 S., 76 Abb., geb., DM 71,90. Chemie Ingenieur Technik, 53(3): 225-225. Portico. https://doi.org/10.1002/cite.330530323
[27] Alnakeeb, M.A., Saad, M.A., Hassab, M.A. (2021). Numerical investigation of thermal and hydraulic performance of fin and flat tube heat exchanger with various aspect ratios. Alexandria Engineering Journal, 60(5): 4255-4265. https://doi.org/10.1016/j.aej.2021.03.036
[28] Launder, B.E., Spalding, D.B. (1983). The numerical computation of turbulent flows. Numerical Prediction of Flow, Heat Transfer, Turbulence and Combustion, 96-116. https://doi.org/10.1016/b978-0-08-030937-8.50016-7
[29] Wesseling, P. (2009). Iterative methods. Springer Series in Computational Mathematics, 263-303. https://doi.org/10.1007/978-3-642-05146-3_7
[30] Zienkiewicz, O.C., Taylor, R.L., Zhu, J.Z. (2013). The Finite Element Method: Its Basis and Fundamentals. https://doi.org/10.1016/b978-1-85617-633-0.00020-4
[31] Ahmed, A.H., Zaidan, M.H., Al-Jethelah, M.S.M. (2023). Aheat transfer and fluid flow characteristics in a TBHE based on constructal design: An overview. NTU Journal of Renewable Energy, 4(1): 57-96. https://doi.org/10.56286/ntujre.v4i1.428
[32] Stanescu, G., Fowler, A.J., Bejan, A. (1996). The optimal spacing of cylinders in free-stream cross-flow forced convection. International Journal of Heat and Mass Transfer, 39(2): 311-317. https://doi.org/10.1016/0017-9310(95)00122-p
[33] Yehia Abbas, N., Waheed Mustafa, A., Kheir Aldeen Abbas Asker, M. (2020). Constructal design of longitudinally finned tubes cooled by forced convection. Heat Transfer, 49(3): 1613-1631. https://doi.org/10.1002/htj.21681
[34] Razera, A.L., Quezada, L.A., Fagundes, T.M., Isoldi, L.A., dos Santos, E.D., Biserni, C., Rocha, L.A.O. (2019). Fluid flow and heat transfer maximization of elliptic cross- section tubes exposed to forced convection: A numerical approach motivated by Bejan's theory. International Communications in Heat and Mass Transfer, 109: 104366. https://doi.org/10.1016/j.icheatmasstransfer.2019.10436

6
[35] Tahseen, T.A., Ishak, M., Rahman, M.M. (2014). An experimental study of heat transfer and friction factor characteristics of finned flat tube banks with in-line tubes configurations. Applied Mechanics and Materials, 564: 197-203. https://doi.org/10.4028/www.scientific.net/AMM.564.197
[36] Liu, X., Yu, J., Yan, G. (2016). A numerical study on the air-side heat transfer of perforated finned-tube heat exchangers with large fin pitches. International Journal of Heat and Mass Transfer, 100: 199-207. https://doi.org/10.1016/j.ijheatmasstransfer.2016.04.081
[37] Anand, N.K., Kim, S.H., Fletcher, L.S. (1992). The effect of plate spacing on free convection between heated parallel plates. Journal of Heat Transfer, 114(2): 515-518. https://doi.org/10.1115/1.2911306
[38] Knight, R.W., Goodling, J.S., Hall, D.J. (1991). Optimal thermal design of forced convection heat sinks-analytical. Journal of Electronic Packaging, 113(3): 313-321. https://doi.org/10.1115/1.2905412
[39] Bejan, A., Sciubba, E. (1992). The optimal spacing of parallel plates cooled by forced convection. International Journal of Heat and Mass Transfer, 35(12): 3259-3264. https://doi.org/10.1016/0017-9310(92)90213-c
[40] Ledezma, G., Morega, A.M., Bejan, A. (1996). Optimal spacing between pin fins with impinging flow. Journal of Heat Transfer, 118(3): 570-577. https://doi.org/10.1115/1.2822670
[41] Fowler, A.J., Ledezma, G.A., Bejan, A. (1997). Optimal geometric arrangement of staggered plates in forced convection. International Journal of Heat and Mass Transfer, 40(8): 1795-1805. https://doi.org/10.1016/s0017-9310(96)00251-7
[42] De, S. (2022). Verification and validation in computational mechanics. Mechanical Engineering, Preprints, 2022020121. https://doi.org/10.20944/preprints202202.0121.v1
[43] Oberkampf, W.L., Roy, C.J. (2010). Verification and Validation in Scientific Computing. Cambridge University Press, 250-285. https://doi.org/10.1017/cbo9780511760396.011
[44] Tahseen, T.A., Ishak, M., Rahman, M.M. (2012). A numerical study of forced convection heat transfer over a series of flat tubes between parallel plates. Journal of Mechanical Engineering and Sciences, 3: 271-280. https://doi.org/10.15282/jmes.3.2012.3.0025
[45] Jang, J.S.R. (1993). ANFIS: adaptive-network-based fuzzy inference system. IEEE Transactions on Systems, Man, and Cybernetics, 23(3): 665-685. https://doi.org/10.1109/21.256541
[46] Ahmad, S., Ullah, A., Ullah, A., Akgül, A., Abdeljawad, T. (2021). Computational analysis of fuzzy fractional order non-dimensional Fisher equation. Physica Scripta, 96(8): 084004. https://doi.org/10.1088/1402-4896/abface
[47] Dayan, F., Ahmed, N., Rafiq, M., Akgül, A., Raza, A., Ahmad, M.O., Jarad, F. (2022). Construction and numerical analysis of a fuzzy non-standard computational method for the solution of an SEIQR model of COVID-19 dynamics. AIMS Mathematics, 7(5): 8449-8470. https://doi.org/10.3934/math.2022471
[48] Drake, R.M. (1967). W. M. Kays, Convective Heat and Mass Transfer, 387 pp. McGraw-Hill, New York (1966). International Journal of Heat and Mass Transfer, 10(8): 1131-1132. https://doi.org/10.1016/0017-9310(67)90130-5
[49] Tiwari, G., Bajpai, G. (2023). Vision enabled contagious ward robotic nurse. International Journal of Engineering Applied Sciences and Technology, 7(10): 172-174. https://doi.org/10.33564/ijeast.2023.v07i10.025
[50] Rizal, M., Ghani, J.A., Husni, Husaini. (2018). Design and construction of a strain gauge-based dynamometer for a 3-axis cutting force measurement in turning process. Journal of Mechanical Engineering and Sciences, 12(4): 4072-4087. https://doi.org/10.15282/jmes.12.4.2018.07.0353
[51] Maghsoudali, Y., Rastegarkoutenaei, A., Sahami, M., Bandpy, M.G. (2022). Investigation of the effect of using the finned tubes on the performance of shell and tube heat exchanger by 3D modeling. Journal of Energy Storage, 56: 106031. https://doi.org/10.1016/j.est.2022.106031

NOMENCLATURE

Be	Bejan number
D_h	hydraulic diameter, m
DT	transverse diameter, m
DL	longitudinal diameter, m
H	domain height, m
h	convection heat transfer coefficient
k	thermal conductivity, W/m K
Re	Reynolds number
Nu	Nusselt number
P	dimensionless pressure, Pa
p	pressure, Pa
Pr	Prandtl number
SL	longitudinal pitch, mm
ST	transverse pitch, mm
Ld	downstream fin length
Lu	upstream fin length
T	temperature, °C
u, v	velocities in x and y- directions, m/s
U, V	dimensionless velocities in X and Y direction
x, y	cartesian coordinates, m
X, Y	dimensionless cartesian coordinates
W	width

Greek symbols

α	thermal diffusivity, m^2/s
φ	angle between the fins
θ	dimensionless temperature
μ	dynamic viscosity, Kg/ms
ρ	density, Kg/m^3
∞	ambient condition

Subscripts

n	normal
s	surface

Abbreviation

CFD	computational fluid dynamic
ANFIS	adaptive neuro-fuzzy model

MF	membership function
LFFTB	longitudinally finned flat tube bank
LFFTBHE	longitudinally finned flat tube bank heat exchanger